Electrohydrodynamic flow control

Status report 2007

TOMAS HURTIG

FOI
Defence Research Agency
Defence & Security, Systems and Technology
SE-147 25 Tumba

Phone: +46 8 555 030 00
Fax: +46 8 555 031 00

www.foi.se

FOI-R--2436--SE Technical report
ISSN 1650-1942 December 2007

Defence & Security, Systems and Technology

Titel	Elektrohydrodynamisk flödeskontroll
Title	Electrohydrodynamic flow control
Rapportnr/Report no	FOI-R—2436--SE
Rapporttyp Report Type	Teknisk rapport Technical report
Sidor/Pages	24 p
Månad/Month	December
Utgivningsår/Year	2007
ISSN	ISSN 1650-1942
Kund/Customer	FMV
Forskningsområde Programme area	5. Bekämpning och skydd 5. Strike and Protection
Delområde Subcategory	55 Flygteknik 55 Aeronautics
Projektnr/Project no	E21201
Godkänd av/Approved by	Anders Larsson

FOI, Totalförsvarets Forskningsinstitut
Avdelningen för Försvars- och säkerhetssystem
Grindsjöns forskningscentrum
147 25 Tumba

FOI , Swedish Defence Research Agency
Defence & Security, Systems and Technology
SE-147 25 Tumba

Sammanfattning

Denna rapport beskriver det arbete inom projektet elektrohydrodynamisk flödeskontroll som utförts under 2007. Under året har en hel del arbete lagts ned på att sprida kunskap om ämnet, både inom och utanför FOI i syfte att väcka intresse och knyta kontakter. Den experimentella verksamheten har inletts med en serie försök där olika elektrodmaterial och geometrier provats. Dessa experiment har visat att resultatet, mätt i elektrisk till mekanisk verkningsgrad, är mycket beroende av geometri. Speciellt elektrodernas utformning är av stor betydelse för verkningsgraden.

Nyckelord: Elektrohydrodynamik, flödeskontroll, plasma, aktuator

Summary

This status report describes the work performed on electrohydrodynamic flow control during the year 2007. Much effort has been devoted to the spreading of knowledge, both outside and within FOI with the purpose of creating an interest for the technology and to build a network. Practical work has been initiated through a series of experiments where electrode materials and geometries have been tested. These experiments have shown that the efficiency of the surface mounted plasma actuator is highly dependent on geometry. Especially the electrode geometry is of great importance to the electrical to mechanical efficiency of the actuator.

Keywords: Electrohydrodynamic, flow control, plasma, actuator

Contents

1 Introduction

Electrohydrodynamic flow control represents an area of research that has expanded tremendously during the last five years [1]. Much of the interest stems from the aerodynamics community, where flow control and especially boundary flow control and the possibility of controlling transition to turbulence and separation control are subjects of great interest [2]. AIAA has in fact recently started an entirely new conference dedicated to flow control. The conference is biannual and the 4th Flow Control Conference will be held in June 2008. Many of the past contributions to this conference concern electrohydrodynamic flow control or, alternatively, plasma flow control. The idea behind plasma flow control is to transfer momentum from ions in an electrical discharge to the surrounding air, the fact that the discharge can be made using very flat (flush mounted) electrodes enables momentum addition directly to the boundary layer in a direction that is tangential to the surface on which the 'plasma actuator' is mounted, see Figure 1.1. It is also possible to arrange the electrodes so that momentum is added in a direction normal to the surface. Since there are no moving parts in a plasma actuator and since the actuator is electrically controlled, fast active feedback is possible [3]. For more background and information on the status of this field of research see the literature survey by Hurtig *et.al* [4].

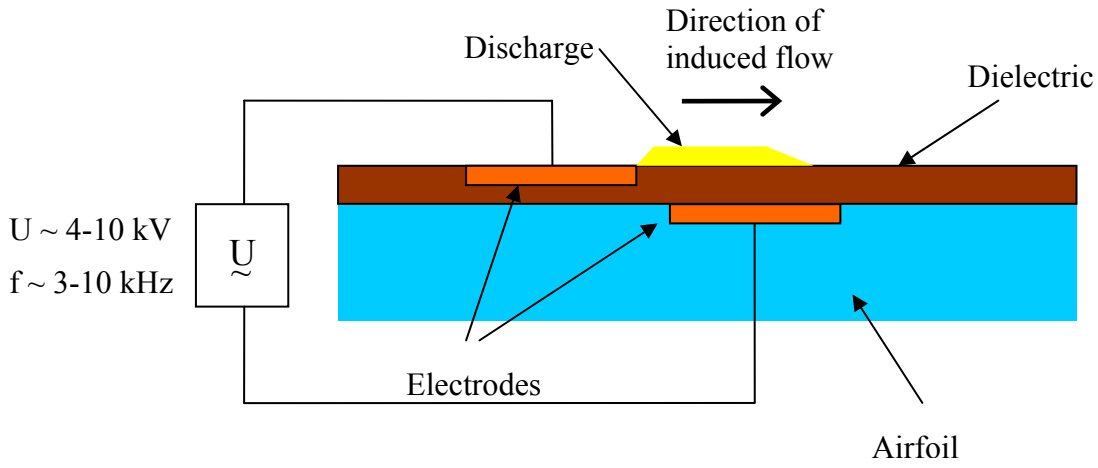

Figure 1.1. Schematic of surface mounted plasma actuator. The actuator consists of two electrodes separated by a dielectric. One electrode is in contact with the surrounding air and theother one is buried under a dielectric surface so that a discharge can be initiated only on the upper surface of the dielectric. This kind of discharge us usually referred to as a Dielectric Barrier Discharge (DBD).

2 Conferences and presentations

During this first year of FOI activity in the area of plasma flow control a lot of work has been devoted to establishing the research area both within FOI itself and externally, in industry and at university. To build competence and interest at FOI a literature survey of the area has been performed and recently published [4]. A presentation of the research area was given at the triannual swedish conference 'Flygteknik 2007' and many new contacts was established through this conference [5]. The research performed at FOI was also presented at an invited seminar at the Alfvén laboratory (Royal Institute of Technology, Stockholm) which is a Swedish competence centre for plasma physics research. An abstract sent to the 2008 ICAS congress (International Council of Aeronautical Sciences) has been accepted and will be presented at the conference in Alaska, USA, 14-16 September 2008.

Contact points and plans for future collaboration in the form of thesis work (Master of Science) have been established with both the Alfvén Laboratory (plasma and discharge physics) and Mälardalen University (aerodynamics).

3 Experiments

A number of different static (no external flow) experiments with plasma actuators have been performed. In all these experiments the plasma actuator consists of two electrodes mounted on each side of a polyimide (Kapton) sheet, unless otherwise noted the thickness of the polyimide film is 127 µm. The trade name of this particular polyimide film is Kapton HN500, see section 7.2. The electrodes are made up of regular copper tape used for screening purposes and usually the bottom electrode is wider than the top electrode. In the very first experiments performed polyimide tape was used (Shercon Inc. #22 Polyimide film tape), see section 7.1. This method was however discarded since this material consists mostly of adhesive (0.04 mm) on a very thin polyimide base (0.03 mm), causing the overall dielectric strength of the material to be determined more by the adhesive than by the polyimide itself. All actuators in this report uses Kapton HN500 for dielectric and two copper tape for electrodes. The bottom electrode is covered with Super Epoxi and a sheet of Kapton CR200 to prevent any plasma formation on the backside of the actuator, for data on CR 200 see section 7.3. A photgraph of a plasma actuator can be seen in Figure 3.1 and a close up of the backside with the electrode edge covered by Epoxi and a strip of CR200 film can be seen in Figure 3.2. The main failure mechanism of these actuators is erosion of dielectric material through interaction of the discharge with the dielectric and heating through mechanical stresses in the dielectric caused by electrical forces on the electrodes. Failure manifests itself in the form dielectric breakdown and subsequent arcing at the breakdown point.

Figure 3.1. Plasma actuator consisting of two electrodes mounted on each side of a 127 µm thick polyimide (Kapton HN500) film. The bottom electrode is covered with Super Epoxi and a sheet of Kapton CR200 to prevent any plasma formation on the backside of the actuator.

Figure 3.2. Close up on backside of plasma actuator. The edge of the bottom electrode is covered with Epoxi glue and a piece of CR200 Kapton covers the edge to prevent any plasma formation. Plasma formation on the 'backside' of the actuator will cause erosion of the surface beneath the actuator, it will also lower the efficiency of the actuator because of the extra energy spent on ionizing the air trapped between the actuator and the surface below.

The plasma actuators used in the experiments reported here can be characterized by a few distinct dimensions, see Figure 3.3. *A* and *B* are the thicknesses of the electrodes and in most experiments we have used ordinary copper tape with a thickness of 70 µm, the horizontal separation between the electrodes, *C*, have been varied between -2 mm (overlapping) and 2 mm. The thickness (*D*) of the dielectric is 127 µm unless otherwise noted.

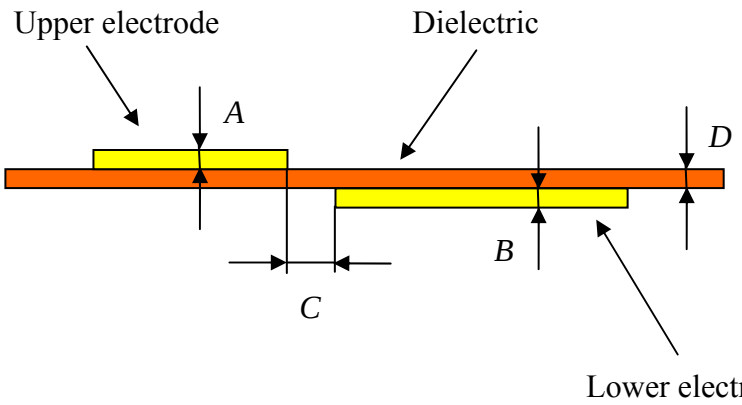

Figure 3.3. Schematic picture of plasma actuator with important dimensions. Typically *A* and *B* are 70 µm, *D* is the thickness of the dielectric and is 127 µm, the distance, *C*, between the edges of the electrodes is usually between -2 mm (overlapping) and 2 mm.

To provide input power to the actuator a signal generator (Rohde&Schwarz 377.5000.02) drives one channel of a high power audio amplifier (Samson SX-3200). The audio amplifier in turn is coupled to a high voltage transformer (Stangenes Inc. SI-16062) that transforms the amplifier output to a high voltage signal that is fed into the plasma actuator, see Figure 3.4.

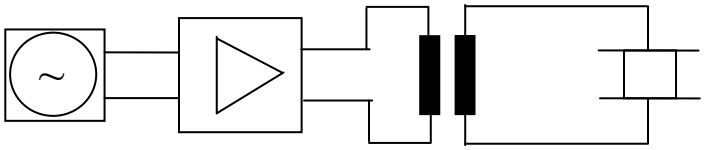

Figure 3.4. Schematic of the experimental setup used in all experiments refrred to in this report. Left to right: signal generator, amplifier, transformer and plasma actuator.

The plasma actuator is a reactive (capacitive) load and as such it is difficult to drive with high efficiency as some of the power in to the device is reflected back. This situation can be improved by inserting an impedance matching network between the amplifier and the transformer or, alternatively, between the transformer and the plasma actuator [6]. An impedance matching network must however be designed to suit a particular plasma actuator at a particular frequency. Since the first part of this project has been devoted to parametric studies of frequency, voltage and actuator geometry, it has not been possible to design an impedance matching network that would suit all the different experiments. When an (in some sense) optimum geometry and frequency is found an impedance matching network will be designed and incorporated into the circuit. It should be noted here that an impedance matching network is only necessary for system (amplifier, transformer and actuator) efficiency. In this report we are only studying the plasma actuator itself, hence there is no need for an impedance matching network at this point.

3.1 Current and voltage characteristics of the plasma actuator

Typical voltage and current traces for plasma actuators can be seen in Figure 3.5. The traces are from two different plasma actuators one with C=0 mm (to the left) and one with C=1 mm. (to the right), illustrated above the experimental data. The traces are taken for an applied voltage of 5 kV and a frequency of 6 kHz on both actuators. Although the current peaks and hence the peak power is much higher for the actuator on the right, the mean power for left hand trace (33 W) is almost double that of the right hand trace (18 W). The polarity in all experiments is positive on the upper electrode that is in contact with air, i.e. when voltage is positive in Figure 3.5 the upper electrode is on higher potential than the lower electrode.

During the negative half cycle the upper electrode is on negative potential relative to the lower electrode and electrons are repelled from the upper electrode and are deposited on the dielectric. When polarity is reversed the electrons deposited on the dielectric in the previous cycle are attracted to the positive upper electrode.

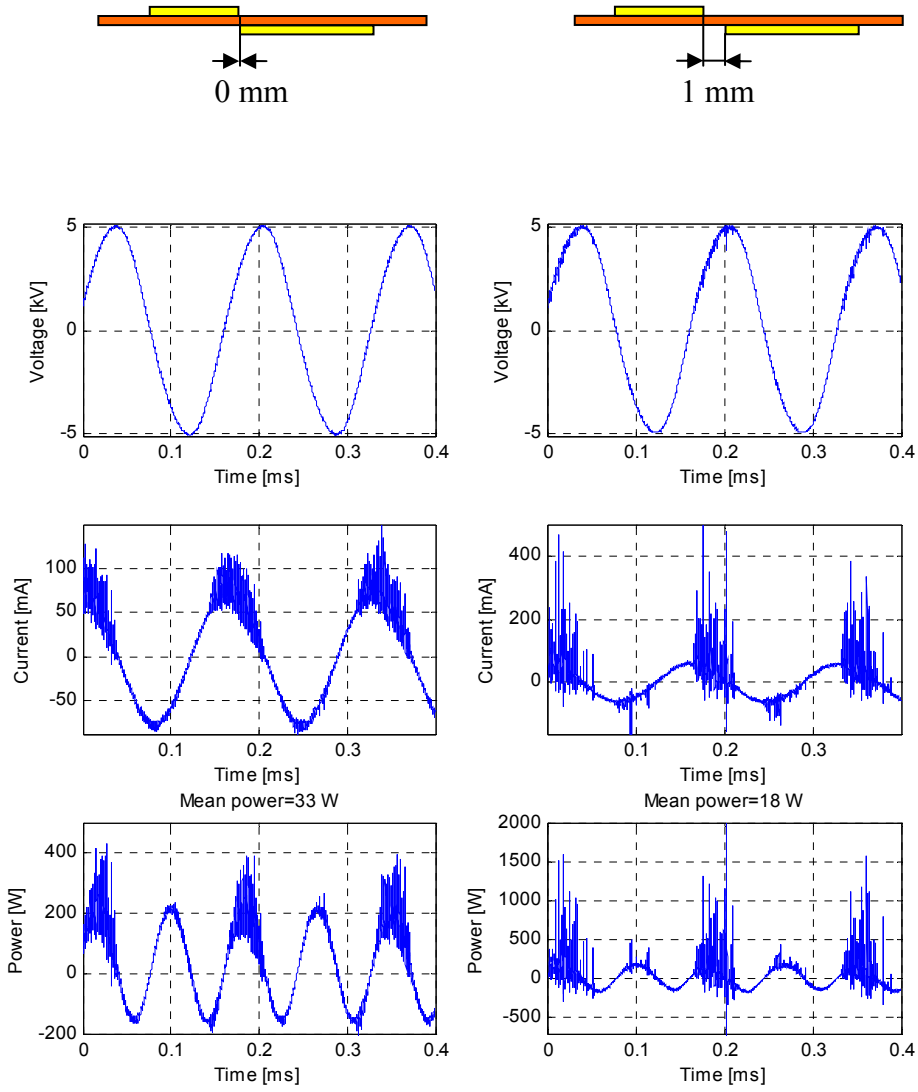

Figure 3.5. Voltage, current and power at an applied voltage of 5 kV plotted as a function of time for two different actuators. The traces on the left are taken from an actuator with electrode separation, *C*, of 0 mm and the traces to the right are from an actuator with electrode separation of 1 mm, see illustration above the experimental data. Although the peak power is much higher for the actuator on the right, the mean power for left hand traces (33 W) is almost double that of the right hand traces (18 W)

3.2 Static experiments

In order to determine what mode of operation that is most efficient in terms of momentum transfer a series of static experiments was performed. In these experiments the surrounding air is at rest and the momentum transfer from the actuator is estimated by measuring the speed of the air flow induced by the actuator itself. The experiment measures an integrated value of the

induced velocity by means of a small 1.5 mm radius hot ball probe placed in the throat of a small wind tunnel experiment.

3.2.1 Static wind tunnel experiments

A small wind tunnel was constructed and built for these experiments, see Figure 3.6. The plasma actuator is placed in the wind tunnel opening (to the left in the picture) and measurements of the induced velocity are made in the exit throat (to the right on the picture). The inside width of the tunnel at the place where the actuator is situated is 320 mm and the height of the tunnel is 10 mm, the width of the exit throat is 15 mm.

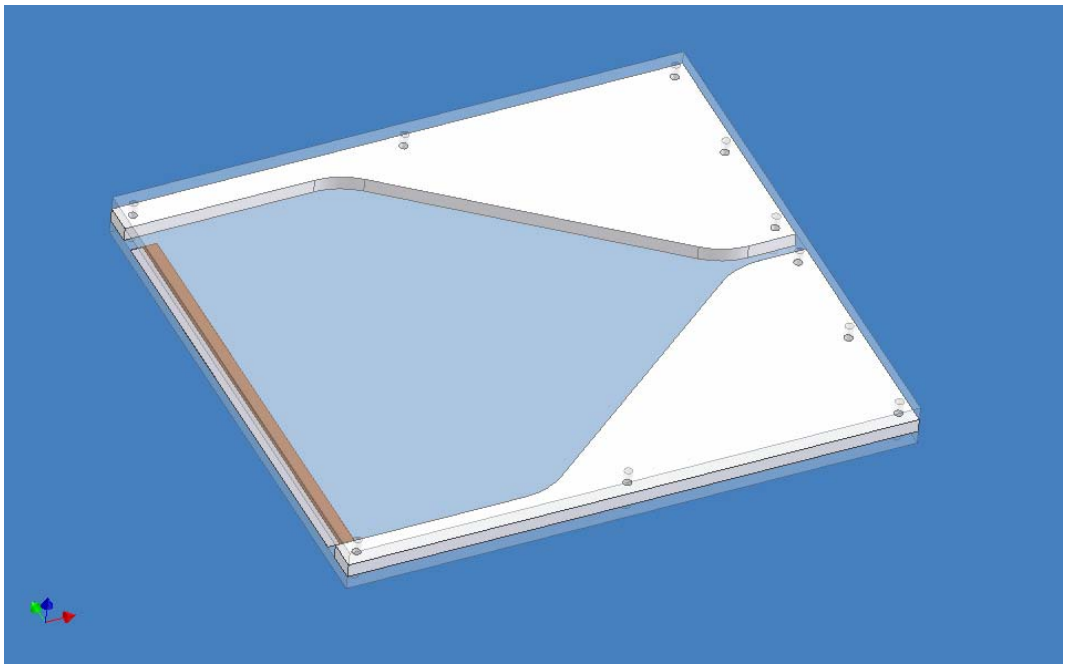

Figure 3.6. 3D drawing of wind tunnel for static plasma actuator experiments. The plasma actuator is placed in the wind tunnel opening (to the left in the picture) and measurements of the induced velocity are made in the exit throat (to the right on the picture). The inside width of the tunnel at the place where the actuator is situated is 320 mm and the height of the tunnel is 10 mm.

The air velocity induced by the actuator is measured by means of a hot ball probe (testo 0628 0035) connected to a measuring transducer (testo 0699 5100/10) that sends an analog signal (1-10 V) to a Fluke multimeter (Fluke 45) that indicates air velocity (0-10 m/s) with a 0.03 m/s resolution. Voltage across the actuator is measured by means of an ordinary voltage divider (1:1000) and current is measured by means of a current probe (Tektronix TM502A). The voltage applied across the plasma actuator and the current flowing through it is recorded on a digital LeCroy oscilloscope (9304M). The experimental setup can be seen in Figure 3.7. A close up on the static wind tunnel and the plasma actuator can be seen in Figure 3.8.

Typical air velocities measured in the output throat of the wind tunnel is on the order of one meter per second, at this stage we are however mostly concerned with relative measurements. It should also be noted here that the velocity measurements have large uncertainties, the reading from the hot ball probe takes several seconds (~5 s) to stabilize and if the actuator is left running for a long enough time the dielectric will start to heat up and this will affect the velocity measurement. Usually the reading from the hot ball probe is taken after the last relevant digit (0.01 m/s) has stabilized for at least three seconds.

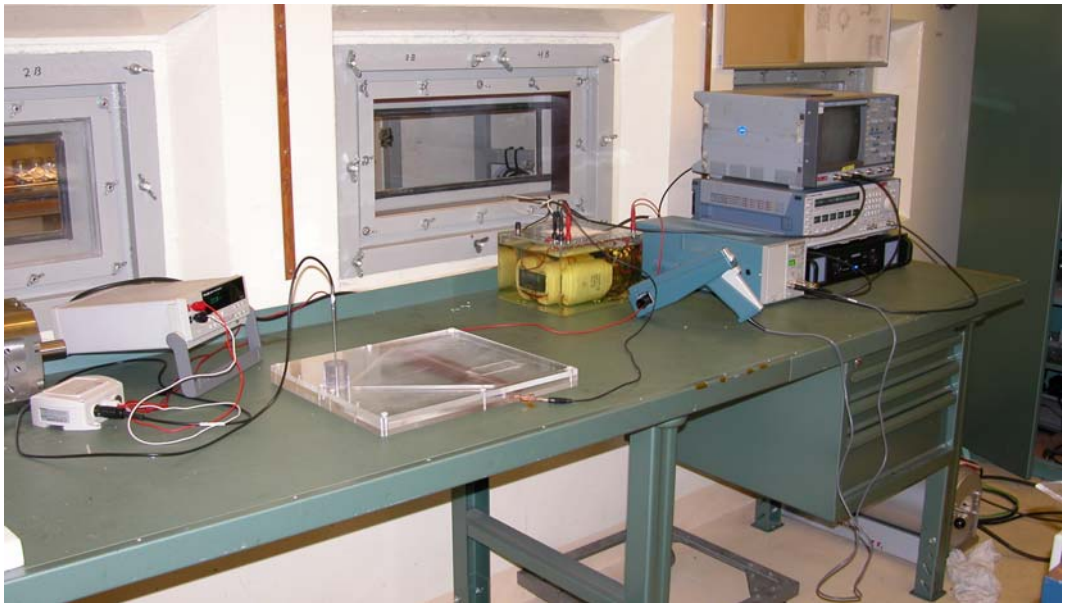

Figure 3.7. Experimental setup used for the static wind tunnel experiments.

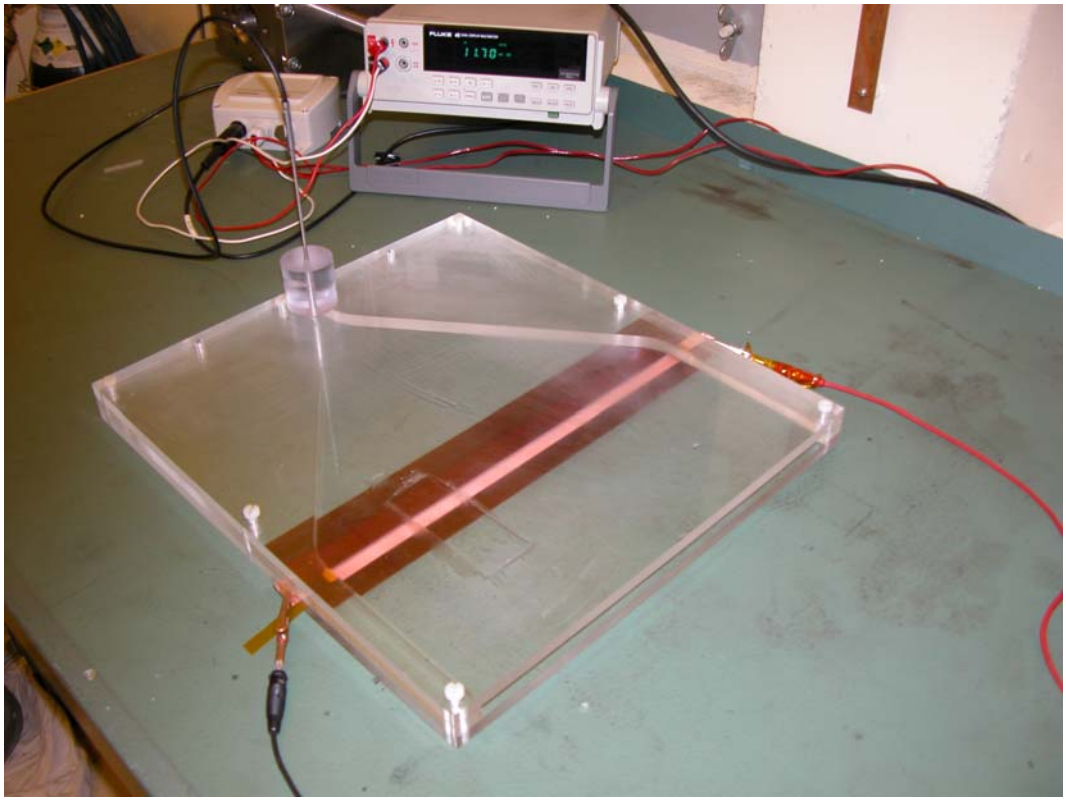

Figure 3.8. Close up on wind tunnel and actuator. The actuator is glued to the bottom plate by the use of photo mount spray glue. The hot ball probe is connected to a signal transducer that gives an output signal 0-10 V corresponding to a measured air velocity of 0-10 m/s. The output from transducer is measured by the Fluke 45 multimeter seen in the background.

Experiments where performed on actuators with different electrode overlapping (dimension *C* in Figure 3.3) and the average velocity of the air in the throat of the wind tunnel was measured for different applied voltages and frequencies for each actuator. Results from experiments on an actuator with *C*=0 mm can be seen in Figure 3.9 where normalized velocity

has been plotted against electrical power per meter actuator for four different applied voltages. At a given voltage level the frequency was varied and as the frequency increase so does the electrical power into the actuator. At the beginning and end of each line the start and end frequencies are noted, see Figure 3.9. We see that air velocity generally increases with increasing voltage and frequency and, hence, input power. It is interesting to note that this trend is actually broken when the 4.5 kV line shows higher air velocity than the 5 kV line at the same input power. This is not completely unexpected since each actuator should have an efficiency peak at some combination of voltage and frequency.

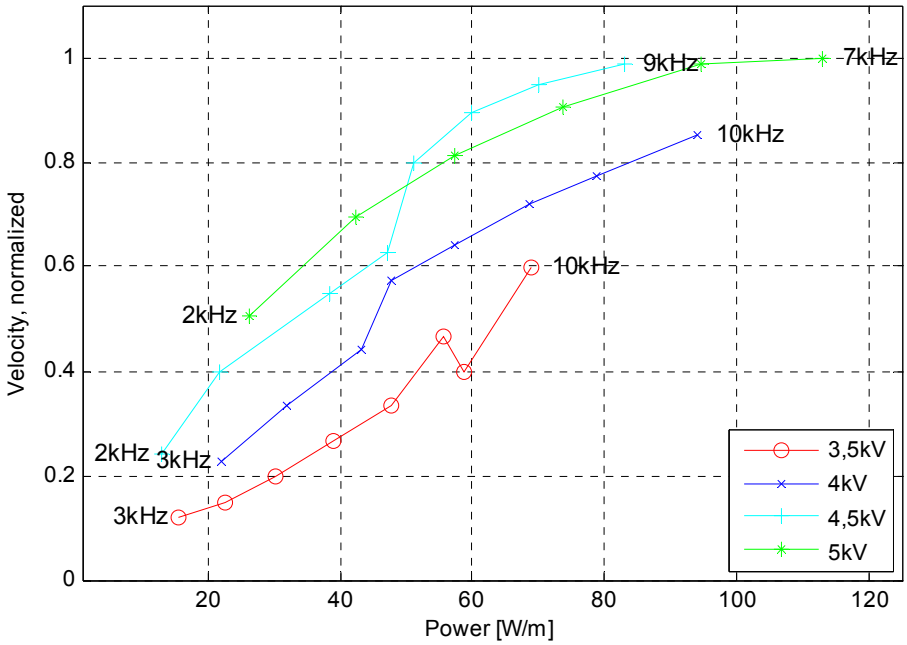

Figure 3.9. Normalized velocity plotted against electrical power per meter actuator (C=0 mm) for four different applied voltages. The frequency was varied between 3 and 10 kHz in all experiments except for the one at 5 kV where the frequency was varied between 2 and 7 kHz. We see that air velocity generally increases with increasing voltage and frequency and, hence, input power. It is interesting to note that this trend is actually broken when the 4.5 kV line shows higher air velocity than the 5 kV line at the same input power.

A true measure of the relative efficiency is obtained if the cube of the velocity (corresponding to power in the airflow) is divided by the electrical power into the actuator. In Figure 3.10 the same data as in Figure 3.9 is plotted but in terms of normalized v^3/P_E versus electrical input power, P_E. Here it is clearly seen that the actuator exhibits regions of highest efficiency both for 5 and 4.5 kV input voltage where the highest efficiency is obtained for 4.5 kV input voltage at about 9 kHz. Note that, for a certain actuator, the most efficient region of operation does not coincide with the highest possible air flow velocity, which is a fact that is often overlooked in the literature. The fact that a certain combination of applied voltage and frequency is more efficient than other combinations seem to support an idea put forward by J. Reece Roth [7, 8]. Roth suggested that the driving voltage and frequency be chosen so that an ion created close to one electrode does not have time to travel across the discharge gap before the voltage reverses, whereas the electrons on the other hand should have time to travel across the gap before the voltage reverse. This ‘ion trapping’ theory is not supported by rigorous theory and has been subjected to some critique, especially for larger electrode gaps (>3 mm) [9]. It is however not unlikely that, for a given applied voltage and geometry, there does indeed exist an ideal driving frequency.

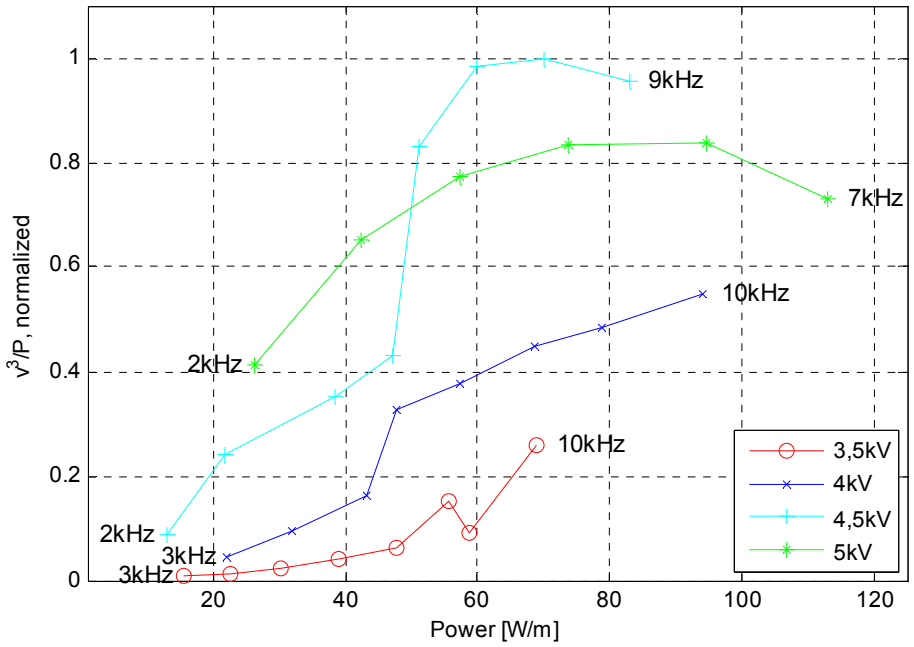

Figure 3.10. The same data as in Figure 3.9 but plotted in terms of normalized v^3/P_E versus electrical input power, P_E. Here it is clearly seen that the actuator exhibits regions of highest efficiency both for 5 and 4.5 kV input voltage where the highest efficiency is obtained for 4.5 kV input voltage at about 9 kHz.

For an actuator with larger horizontal separation between the electrodes (C=1 mm) the region of highest efficiency is shifted towards larger input power, see Figure 3.11 and Figure 3.12. The drop in velocity that can be seen for the highest input powers (5.5 kV at 170 W) can be due to heating of the dielectric material and subsequent heating of the air flowing above the plasma actuator and thus an error in the measurement taken with the hot ball probe. The low flow speeds measured at an applied voltage of 4.5 kV are due to the fact that the discharge is barely established at this low voltage. For higher applied voltage (5 and 5.5 kV) this actuator exhibits the same general trend as the actuator with C=0 mm, i.e. the region of most efficient operation move towards higher power (and frequency) when the voltage is increased.

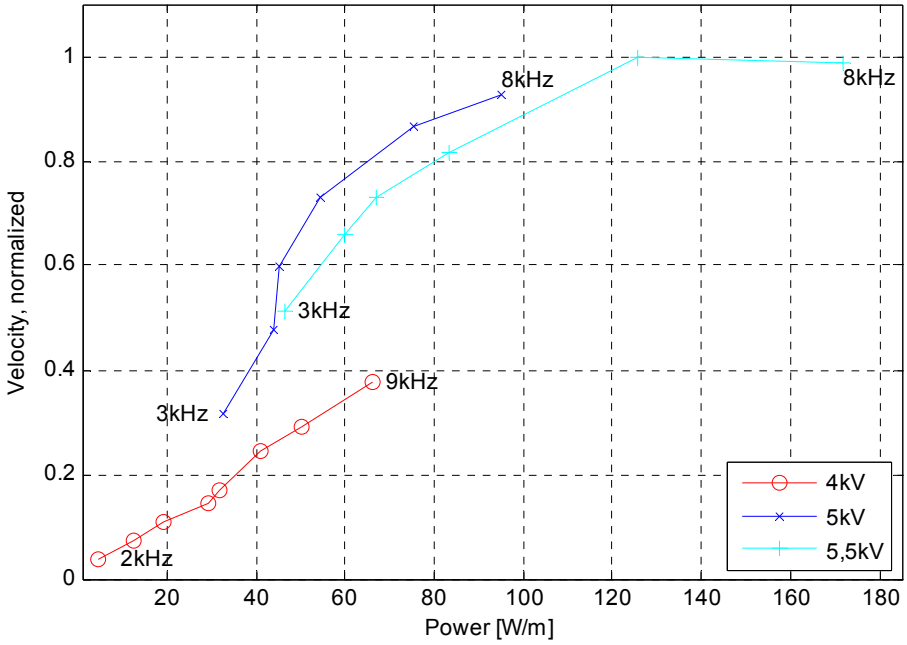

Figure 3.11. Normalized velocity plotted against electrical power per meter actuator (C=1 mm) for three different applied voltages. The drop in velocity at the highest input power (170 W) can be due to heating of the air stream when it passes the actuator and thus an error in the measurement by the hot ball probe.

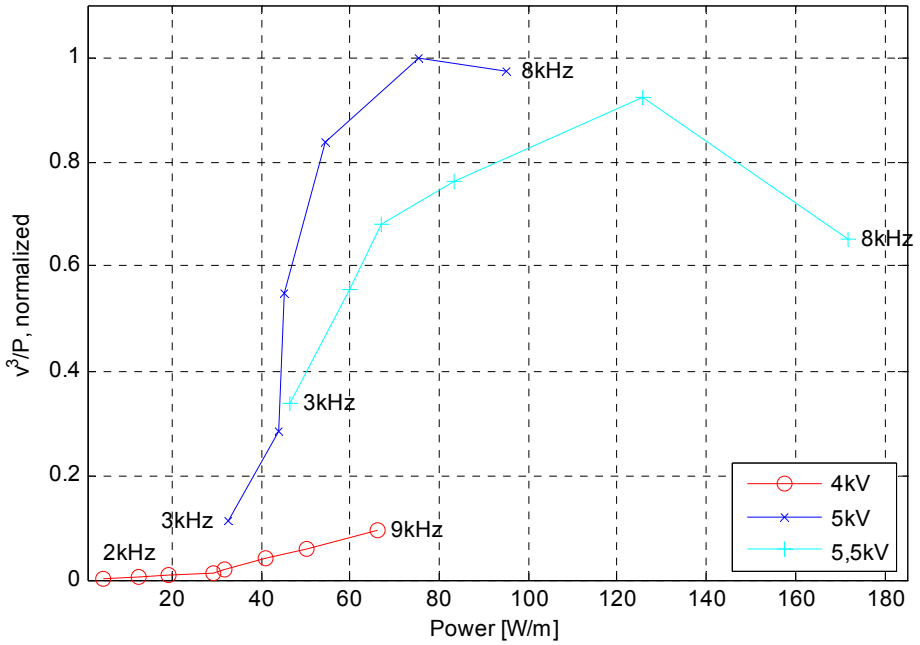

Figure 3.12. The same data as in Figure 3.11 but plotted in terms of normalized v^3/P_E versus electrical input power, P_E. Here it is clearly seen that the actuator exhibits regions of highest efficiency both for 5 and 5.5 kV input voltage where the highest efficiency is obtained for 5 kV input voltage at about 7 kHz.

The effect of electrode thickness was investigated by replacing the fairly thick (70 µm) copper tape with very thin (15 µm) aluminum foil that was glued, using Super Epoxi, onto the Kapton film. Following the notation introduced in Figure 3.3 the data for this actuator was A=B=15 µm and C=1 mm. The use of the very thin aluminum foil made it more difficult to find an optimum operating mode, see Figure 3.13 and Figure 3.14, below. The very sharp peak in the data taken at an applied voltage of 4.5 kV needs to be investigated further and the strange behavior (with two peaks) in the 5.5 kV curve also needs closer attention, see Figure 3.14. We also note that even at fairly low applied voltages (4.5 kV) the efficiency is comparable to the efficiency at higher voltage, which is not the case for actuator with copper electrodes and 1 mm spacing (C=1 mm) . This is probably due to the fact that, for a certain applied voltage, the thinner aluminum foil will cause a higher local electric field than the thicker copper electrode. Hence plasma production will begin at a lower value of applied voltage for the (thin) aluminum foil actuator than for the (thick) copper foil actuator. This experiment should be repeated with thin copper foils to rule out any dependence on electrode material.

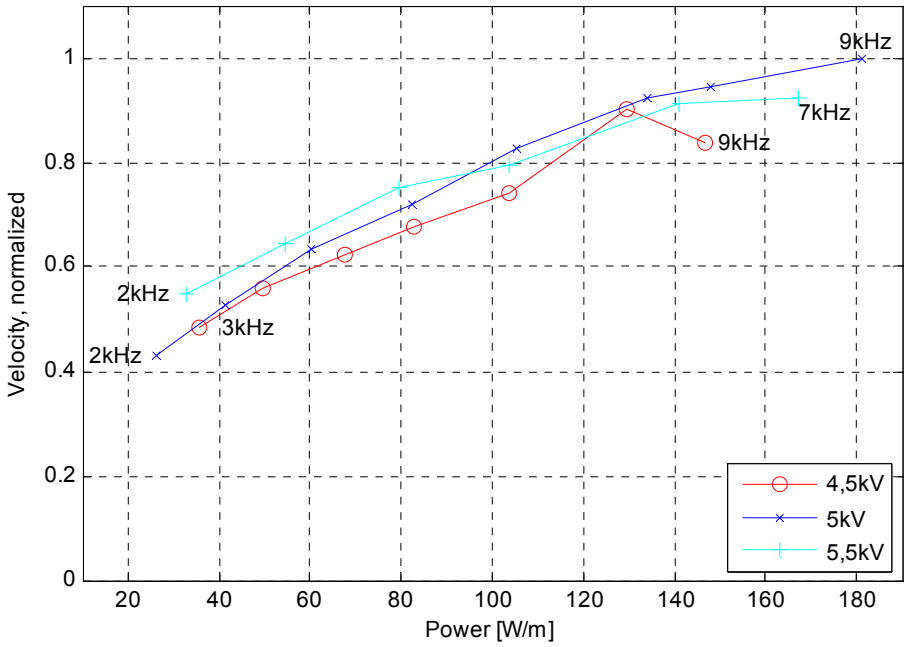

Figure 3.13. Normalized velocity as a function of input power for an actuator with 15 µm thick aluminum electrodes. This actuator exhibits a more uniform behavior than the actuators with copper electrodes.

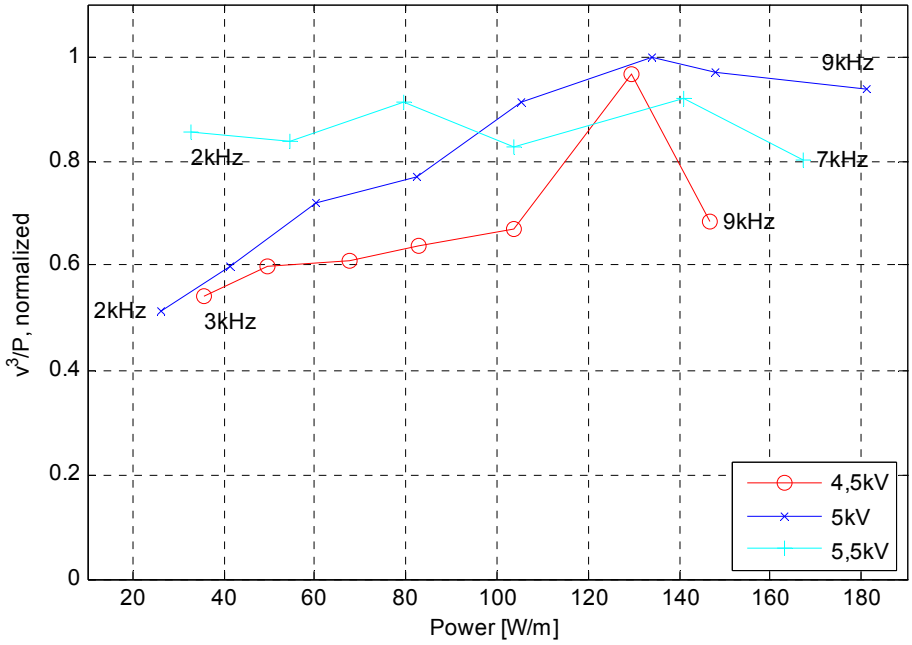

Figure 3.14. The same data as in Figure 3.13 but with normalized efficiency plotted against input power per meter actuator. The 4.5 kV trace shows a very sharp peak in efficiency at 8 kHz and about 130 W input power. The 5.5 kV trace seems two have two, not so distinct, efficiency peaks at 80 and 140 W input power. Both of these observations call for further investigations in order to determine the cause for the rather strange behavior.

The effect of increasing the local electric field for a given applied voltage can be further increased by using even thinner electrodes. Consequently the upper electrode was replaced with a carbon fiber 'comb', see Figure 3.15, where each fiber has a diameter of about 7 µm. As expected this method generates a plasma at very low values of applied voltage, unfortunately it did not perform well in terms of electric to mechanical power efficiency. The investigation into using carbon fiber electrodes is still under way and the results are not fully analyzed yet. One possible reason for the poor efficiency of these electrodes is that the comb is quite thick, and consequently the air has to pass through the upper layer of fibers before it reaches the discharge region where it is accelerated. The discharge has to suck the air through a dense carbon fiber brush. Future experiments will use brushes with only a thin layer of carbon fiber.

Figure 3.15. Upper electrode replaced with a carbon fiber 'comb', to increase the effect of electric field enhancement. Each fiber in the comb has a diameter of 7 µm. Bottom electrode (aluminum) is visible through the Kapton dielectric.

4 Theory and simulation work

The theory for electrical discharges at atmospheric pressure and its interaction with a surrounding air flow is very complex and usually a number of simplifications are made in order to reduce the problem to a manageable size. Different researchers make different assumptions and in the area of plasma flow control theory and simulation no consensus has been reached. For this reason a theoretical investigation into the continuum mechanical methods for partially ionized mixtures was performed. This investigation can form the basis of future computational studies of plasma actuators and their interaction with the external flow. Some work concerning the implementation of a numerical description has been started but has not yet produced any publishable results.

5 Future work

The immediate plans for future experimental work involve the testing of different electrode and dielectric materials such as carbon fiber brushes and Teflon, and PVC dielectrics. Plans have also been made to perform simple, small scale, wind tunnel tests at FOI's wind tunnel test facilities at Bromma. Measurements of velocity profile and skin friction on a flat plate are planned for the end of 2007 or beginning of 2008.

Electrohydrodynamic flow control has great potential as an alternative and/or complement to established boundary layer flow control techniques. Because of the absence of moving parts that enables the use of fast active feedback and other advanced control strategies, the plasma actuator and its ability to add momentum directly to the boundary layer is a very interesting technique. However, based on the experience from the first year of research into the subject of electrohydrodynamic flow control we feel that there are two main issues that need to be resolved before the plasma actuator is a serious competitor to other, established, boundary flow control techniques. One issue is the dielectric strength of the materials used. The other issue is the efficiency in terms of electrical to mechanical power conversion which is still very low (< 1 %). For this reason future work will be concentrated towards finding new materials and new combination of materials that are less prone to dielectric breakdown and towards a better understanding of the atmospheric pressure discharge physics responsible for momentum transfer from ions to surrounding air. When a better understanding of the underlying physics is reached an optimization of the plasma actuator will be possible.

6 References

1. Roth, J.R., *Physics and phenomenology of plasma actuators for control of aeronautical flows.* Journal of Physics D, 2007. **40**.
2. Gad-el-Hak, M., *Flow Control: Passive, Active, and Reactive Flow Management*. 2000: Cambridge University Press.
3. Brandon L. Snyder, et al. *Closed-Loop Plasma Active Control Technology (CLOPACT).* in *45th AIAA Aerospace Sciences Meeting and Exhibit*. 2007. Reno, Nevada.
4. Tomas Hurtig, Anders Larsson, and M. Liefvendahl, *Electrohydrodynamic Flow Control - A litterature Survey*. 2007.
5. Tomas Hurtig, Anders Larsson, and E. Prisell. *Elektrohydrodynamisk flödeskontroll*. in *Flygteknik 2007*. 2007. Stockholm City Conference Centre - Norra Latin, Stockholm, Sweden.
6. Chen, Z., *Impedance Matching for One Atmosphere Uniform Glow Discharge Plasma (OAUGDP) Reactors.* IEEE Transactions on Plasma Science, 2002. **30**(5).
7. J.Reece Roth, Daniel M. Sherman, and S.P. Wilkinson. *Boundary Layer Flow Control with a One Atmosphere Uniform Glow Discharge Surface Plasma*. in *36th Aerospace Sciences Meeting and Exhibit*. 1998. Reno, Nevada.
8. Roth, J.R., *Industrial Plasma Engineering*. Vol. 2. 2001: IOP.
9. Xinxin Wang, et al., *Study on an atmospheric pressure glow discharge.* Plasma Sources Sci. Technology, 2003. **12**: p. 358-361.

7 Appendix

7.1 Data for Kapton tape

#22 Polyimide film tape. Data and Specification Sheet.

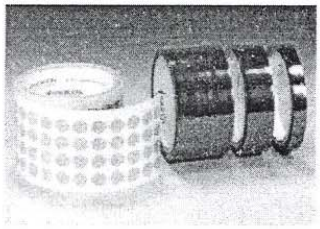

Description
This high temperature film tape is used in electrical and thermal insulation, in particular in the masking of Gold fingers on circuit boards during wave soldering. It's excellent release properties, also mean it can be used in the powder coating industries.

Construction

Description	Value	ASTM Test method
Film thickness	1.0 Mil (0.03 mm)	D-3652
Adhesive thickness	1.5 Mil (0.04 mm)	D-3652
Total thickness	2.5 Mil (0.07 mm)	D-3652
Color	Amber	
Adhesive	Crosslinked silicone	
Breaking strength	30lb. / Inch (5.4Kg. / cm)	
Elongation at break	60%	D-3759
Adhesion to steel	26 oz. / inch (0.3Kg / cm)	D-3330
Dielectric Strength	7,500 Volts	
Insulation Class	356°F (180°C)	
Temperature range	-100°F to 500°F (-73°C to 260°C). This tape will withstand short term, intermittent temperatures to 600°F (315°C)	
Storage conditions	keep in dry conditions	
Removability	Good to Excellent	
Shear strength	Very high, even at high temperatures	
Tack	Moderate to Excellent	
Humidity resistance	Very good	
UV resistance	Good	
Tolerance	Discs and die cuts can be cut to a tolerance of +/-0.005" (+/-0.127mm)	

Availability
Available in roll form in a range of imperial and metric widths. This tape is also available in pre-cut disc sizes in both imperial and metric diameters. Alongside this, it can be provided in rectangular cutoff form or as die cut shapes.

General applications
This tape offers optimum performance in electrical and thermal insulation. It offers flame resistant electrical insulation, can be used as a wire and cable wrap, as well as for solder masks for circuit boards.

SHERCON, INC. TECHNICAL INFO PACK 65
ISSUE 1. JUN. 12, 98

7.2 Electrical data for Kapton HN

Typical Electrical Properties of Kapton® HN Film at 23°C (73°F), 50% RH

Property Film Gage	Typical Value	Test Condition	Test Method
Dielectric Strength 25 µm (1 mil) 50 µm (2 mil) 75 µm (3 mil) 125 µm (5 mil)	V/m kV/mm (V/mil) 303 (7700) 240 (6100) 205 (5200) 154 (3900)	60 Hz 1/4 in electrodes 500 V/sec rise	ASTM D-149-91
Dielectric Constant 25 µm (1 mil) 50 µm (2 mil) 75 µm (3 mil) 125 µm (5 mil)	 3.4 3.4 3.5 3.5	1 kHz	ASTM D-150-92
Dissipation Factor 25 µm (1 mil) 50 µm (2 mil) 75 µm (3 mil) 125 µm (5 mil)	Ω 0.0018 0.0020 0.0020 0.0026	1 kHz	ASTM D-150-92
Volume Resistivity 25 µm (1 mil) 50 µm (2 mil) 75 µm (3 mil) 125 µm (5 mil)	•cm 1.5×10^{17} 1.5×10^{17} 1.4×10^{17} 1.0×10^{17}		ASTM D-257-91

7.3 Data for Kapton CR

Typical Properties of Kapton® Type 150 FCR 019 Polyimide Film, 37.5 µm (1.5 mil)

Property	Typical Value at 23°C (73°F)	Test Method
Electrical		
Corona Resistance, hr at 20 kV/mm at 50 Hz	>100,000	IEC-343
Dielectric Strength, kV/mm (V/mil)	173 (4,400)	ASTM D-149-81
Dielectric Constant	2.9	ASTM D-150-81
Dissipation Factor	0.001	ASTM D-150-81
Volume Resistivity, ohm·cm	5.3×10^{16}	ASTM D-257-78
Surface Resistivity, ohm/sq	1.6×10^{15}	ASTM D-257-78
Mechanical		
Ultimate Tensile Strength, MPa (psi)	117 (17,000)	ASTM D-882-91
Yield Point at 3%, MPa (psi)	48 (7,000)	ASTM D-882-91
Stress to Produce 5% Elongation, MPa (psi)	62 (9,000)	ASTM D-882-91
Ultimate Elongation, %	43	ASTM D-882-91
Tensile Modulus, GPa (psi)	2.4 (348,000)	ASTM D-882-91
Tear Strength—Propagating, N (lbf)	0.05 (0.012)	ASTM D-1922
Tear Strength—Initial, N (lbf)	5.3 (1.2)	ASTM D-1004-90
Density, g/cm³	1.72	ASTM D-1004-90
Yield, m²/kg (ft²/lb)	15.79 (77.4)	—
Bonding, N/cm (lb/in)		
Teflon® FEP to Kapton® CR	7.7 (4.4)	DuPont Test
Teflon® FEP to Copper	7.9 (4.5)	DuPont Test
Laminate Bond as Received	1.2 (0.7)	DuPont Test